npj | precision oncology

Article

Published in partnership with The Hormel Institute, University of Minnesota

https://doi.org/10.1038/s41698-025-00926-5

SHMT inhibitor synergizes with 5-Fu to suppress gastric cancer via cell cycle arrest and chemoresistance alleviation

Huan Deng, Yajie Wang, Lin Xiao, Mei Feng, Weidong Dou & Yisheng Pan

Advanced gastric cancer (GC) represents a malignancy tumor with poor prognosis, which requires urgent exploration into its molecular drivers and innovative therapeutic strategies. This study investigates the oncogenic role of serine hydroxymethyltransferase isoforms (SHMT1/SHMT2), key regulators of serine-glycine-one-carbon metabolism, in GC progression and chemoresistanc. Bioinformatics analysis and cytological experiments preliminary identified the important role of SHMTs in GC. Drug synergistic screening assays were used to build the therapeutic model in the study. The transcriptomic analysis was performed to clarify the underlying mechanism of combination treatment. Our investigations demonstrate that SHMT1 and SHMT2 functionally drive malignant progression and confer 5-fluorouracil (5-Fu) resistance in GC, while their selective inhibitor SHIN1 emerges as a novel therapeutic candidate for GC treatment. The synergistic screening analysis showed that SHIN1 was an efficient synergist for 5-Fu, and the combinative therapy amplified their anticancer effects. Mechanistically, the combination treatment induced cell cycle arrest, DNA damage and cellular senescence by regulating the P53 signaling pathway. These unique characteristics of cell cycle arrest through interfering nucleotide synthesis were validated by substantial in vitro and in vivo assays. The present study revealed SHMT isforms as the potential promoter for malignant progression and chemoresistance in GC. The inhibitor SHIN1 alleviates chemoresistance of 5-Fu and augments both therapeutic effects on GC. In conclusion, the combination of SHIN1 with 5-Fu represents a promising preclinical model for GC treatment, offering a novel strategy to overcome drug resistance and improve therapeutic efficacy.

Gastric cancer (GC) has become one of the most prevalent and aggressive malignancies worldwide. According to the latest epidemiological results, its incidence and mortality rates rank among the top five for cancers[1,2]. Despite notable progress in clinical treatment, the 5-year overall survival (OS) of GC patients is less than 30%. Current treatment strategie cannot completely prevent the malignant progression of GC, contributing significantly to the poor prognosis of patients. The pathogenesis and molecular evolution of GC are currently unclear, which indicates that these mechanisms have profound significance for the prevention and treatment of GC. There is an urgent need for more efficient targets and markers for the diagnosis and treatment of GC.

Serine hydroxymethyltransferase (SHMT), an essential enzyme in serine-glycine-nucleotide metabolic network, is integral to the onset and progression of tumors[3,4]. SHMT is the key enzyme that mediates the synthesis of glycine from serine and may participate in the malignant development of GC through multiple carcinogenic mechanisms[5]. The two subtypes of SHMT, SHMT1 and SHMT2, are located in the cytoplasm and mitochondria, respectively[6]. Glycine is an important energy source and material basis for cell proliferation, and its metabolism is correlated with one-carbon metabolism (OCM). One-carbon units cannot exist freely in the cellular environment and need to be combined with tetrahydrofolate (THF) as the carrier to generate 5,10-methylenetetrahydrofolate (5,10-MeTHF)[7]. Currently, anticancer drugs such as methotrexate have been developed to target folate and one-carbon metabolism pathways and have demonstrated increased efficacy in the treatment of tumors[8,9]. Therefore, developing anticancer drugs that target the glycine and OCM metabolic pathways is promising for the treatment of GC.

SHMT maintains the malignant biological behaviors of cancers by regulating the metabolism of one-carbon units and glycine. A previous

Department of Gastrointestinal surgery, Peking University First Hospital, 100034 Beijing, China.
e-mail: yisheng.pan@pkufh.com; bdyypanyisheng@163.com

The Hormel Institute
University of Minnesota

study revealed that elevated SHMT expression is associated with malignant progression and predicts poor prognosis in gastrointestinal malignancies[10]. In addition, studies have shown that the absence of SHMT significantly reduces the formation of gastric cancer stem cell (GCSC) spheres and increases the chemotherapeutic sensitivity of gastric cancer cells to 5-fu[11]. These research results prompted us to consider that elucidating the cancer-promoting mechanism of SHMT and exploring targeted drugs could lead to new options for the treatment of GC. The serine hydroxymethyltransferase inhibitor 1 (SHIN1), AGF347 and serine hydroxymethyltransferase inhibitor 2 (SHIN2) has been explored for its use in the treatment of several tumors[12–15]. These inhibitors disrupt glycine synthesis and one-carbon metabolism by inhibiting the expression of two subtypes of SHMT, thereby inhibiting tumor growth[16]. However, the important therapeutic effect of these inhibitors on GC has not been elucidated.

In this study, we uncovered novel mechanisms by which SHMT regulates GC malignant behaviors and explored the function of SHIN1 in the treatment of GC. SHMT regulates the serine–glycine pathway to produce one-carbon units, promoting the synthesis of purine nucleotides and providing a material basis for the proliferation of GC cells. This study focused mainly on the inhibition of SHMT and established an efficient preclinical model for the treatment of GC. Furthermore, these results will provide a solid foundation for early diagnosis, selection of therapeutic regimens and prognostic evaluation.

Results and discussion

SHMT is the potential malignant promoter for gastric cancer

Gene alterations in the glycine-serine KEGG metabolism pathway were frequently observed in GC patients (TCGA database) (Fig. 1A). There was a significant difference in the expression of 31 genes in the pathway between GC tissue and adjacent normal tissues (Fig. 1B). SHMT1 and SHMT2 were significantly upregulated in gastric tumors compared with adjacent normal tissues (Fig. 1C–E). Clinicopathological features of SHMT1 and SHMT2 were correlated with malignant advancement in GC (Tables 1 and 2). Survival analysis revealed that high SHMT expression predicted poor overall survival (OS), disease-free survival (DFS) and progression-free survival (PFS) for patients with GC ($P < 0.05$, Fig. 1F, Supplementary Fig. 1A–D).

Spearman correlation analysis showed a positive correlation between SHMT1 and SHMT2 expression in GC, which may coordinate and promote the progression of gastric cancer (Supplementary Fig. 1E). SHMT2 exhibited a moderate but statistically significant positive correlation with activated dendritic cells (aDCs; $R = 0.139$, $P = 0.007$; Supplementary Fig. 1F), whereas SHMT1 showed no significant association with aDCs ($P = 0.101$; Supplementary Fig. 1G). Notably, SHMT2 demonstrated a moderate pro-angiogenic role through its correlation with vascular endothelial growth factor A (VEGFA; $R = 0.156$, $P = 0.002$; Supplementary Fig. 1H), while SHMT1 displayed a stronger linkage to VEGFA ($R = 0.231$, $P < 0.001$; Supplementary Fig. 1I), suggesting isoform-specific contributions to angiogenesis. Both isoforms converged on robust associations with tumor proliferation, as evidenced by their strong correlations with marker of proliferation Ki-67 (SHMT1: $R = 0.433$, $P < 0.001$, Supplementary Fig. 1J; SHMT2: $R = 0.387$, $P < 0.001$, Supplementary Fig. 1K). Strikingly, SHMT1 uniquely correlated with erb-b2 receptor tyrosine kinase 2 (ERBB2; $R = 0.242$, $P < 0.001$; Supplementary Fig. 1L), whereas SHMT2 showed no significant relationship with ERBB2 ($P = 0.149$; Supplementary Fig. 1M), highlighting SHMT1's preferential involvement in HER2 signaling. These results demonstrate the diverse mechanisms by which the two subtypes of SHMT promote the progression of GC, while inhibiting them may become synergistic therapeutic targets for other clinical drugs.

SHMT promotes the malignant proliferation and migration of gastric cancer cells

The correlation between SHMT expression and the clinical characteristics of GC patients prompted us to speculate on its potential promotion of malignant progression in GC cells. Transcriptomic changes in SHMT1 and SHMT2 were consistently observed across multiple GC cell lines, positioning them as valuable preclinical models for investigating the pharmacological effects of targeted inhibitors and drug screening for combination therapies in GC. Based on the expression status of SHMT in Cancer Cell Line Encyclopedia (CCLE) database (Fig. 1G), we further tested the expression levels of two subtypes of SHMT in several of GC cell lines in our laboratory (Fig. 2A, B). As a result, it was found that there were differences in the expression levels of SHMT1 and SHMT2 in cell lines. Ultimately, based on CCLE data, previous research and the results of our experiment, we comprehensively selected HGC-27 and AGS cell lines with relatively high expression of both SHMT subtypes for subsequent research.

Overexpression plasmids and shRNAs targeting SHMT1/2 were designed and engineered to generate cell lines with stable overexpression or knockdown (Fig. 2C–F). CCK-8 assays indicated that SHMT overexpression increased proliferation in HGC-27 and AGS cells, while SHMT knockdown diminished their growth (Fig. 2G). The results of the colony formation assays were consistent with those of CCK-8 assays (Fig. 2H–J), which indicated that SHMT1 and SHMT2 promoted the proliferation of GC cells. As shown by wound healing assays and transwell assays, overexpression of SHMT facilitates the migration of GC cells. Moreover, the knockdown of SHMT suppressed these abilities in GC (Fig. 2K–N). The above results indicate that SHMT promotes malignant proliferation and migration in GC.

Validation of the effect of SHMTs-targeted inhibitors on GC and screening its synergistic combinative drugs

Previous studies have demonstrated that knockdown of SHMT inhibited the growth of multiple cancers. The targeted inhibitors of SHMT have been developed and explored in the treatment of tumors. We searched published papers and drug databases, the result showed that SHIN1, SHIN2 and AGF347 were mature inhibitors, which can targeted SHMT1 and SHMT2 simultaneously. However, the inhibitory effect of these inhibitors on GC has not yet been elucidated. HGC-27 has relatively significant expression of both SHMT1 and SHMT2, leading us to explore the inhibitory effects of drugs in this cell line. We first explored the inhibitory effect of SHIN1 on HGC-27 cells, and the results showed that the 50% inhibition concentration (IC_{50}) was approximately 30.78 μM (Fig. 3A). The IC50 of SHIN2 and AGF347 were 75.44 μM and 106.6 μM, respectively (Supplementary Fig. 2A-B). This results revealed that SHIN2 and AGF347 had inefficient inhibitory effects on GC cells. CCK-8 assays were conducted to evaluate the inhibitory effects of varying inhibitor doses on GC cell proliferation. The therapeutic effect of SHIN1 on GC elevated with increasing drug concentrations (Fig. 3B). Whereas, the treatment effects of SHIN2 and AGF347 on GC were inefficiency (Supplementary Fig. 2C-D). We further verified the treatment doses of SHIN1 were harmless to normal gastric epithelial cells (Supplementary Fig. 2E). These findings support our investigation into SHIN1 – a dual inhibitor targeting both SHMT1 and SHMT2 subtypes – for GC treatment. Based on the biological mechanism by which SHMT regulates glycine and one-carbon metabolism, we detected the effects of SHIN1 on several related metabolites. When SHIN1 was used in GC cells, we observed an elevation in serine levels and a decline in glycine levels (Fig. 3C). Glycine is the energy source for tumor cells and the basic building block of purine nucleotides. We also observed elevated levels of purine precursors AICAR and GAR, which are involved in the early stages of purine synthesis, where formate and one-carbon units are integrated (Fig. 3C). SHIN1 interferes one-carbon metabolism and possible depletes THF by SHMT1 and SHMT2 inhibition, inducing an metabolic arrest in AICAR and GAR. Furthermore, there was a significant decrease in downstream guanosine monophosphate (GMP) and adenosine monophosphate (AMP) levels (Fig. 3C). We further found that formate rescue of cell growth in SHIN1-treated cells requires glycine, revealing the potential role of SHIN1 in inhibiting nucleotide synthesis and cell growth (Supplementary Fig. 2F-G). The combination of inhibitors with chemical drugs has been applied in the treatment of various cancers. In order to explore high-

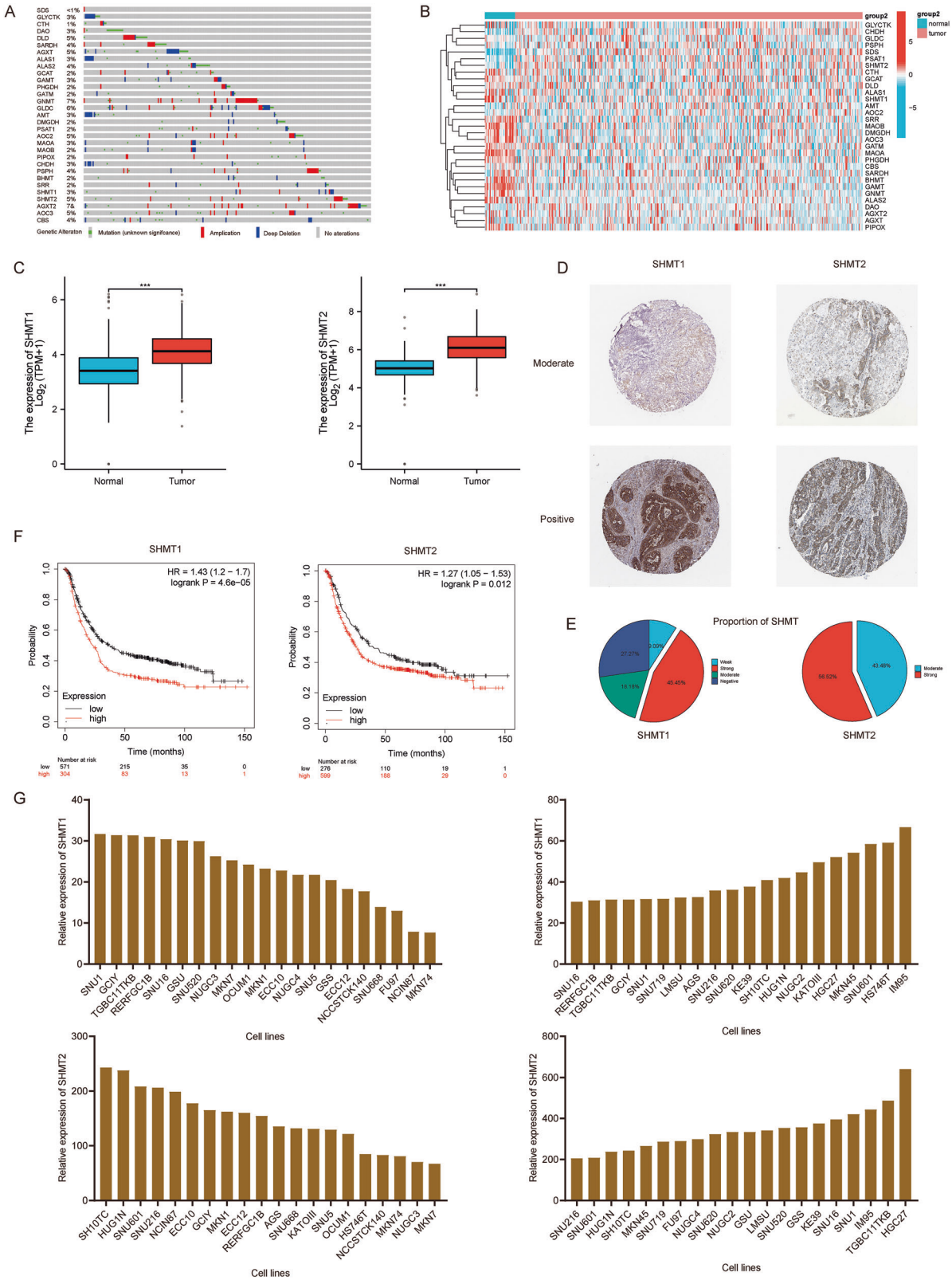

Fig. 1 | SHMT1 and SHMT2 are upregulated in GC and are correlated with poor prognosis. A Percentage of gene aberrations in the KEGG serine-glycine metabolic pathway in the TCGA-STAD cohort (PanCancer Atlas). **B**, **C** Gene expression profiling analysis of TCGA database from the TCGA-STAD cohort showed the expression of SHMT1 and SHMT2 in GC tissues and paired adjacent normal tissues. **D** IHC staining of SHMT1 and SHMT2 in GC tissues from The Human Protein Atlas. **E** The proportions of stained intensity for SHMT1 and SHMT2 from The Human Protein Atlas. **F** Patient survival data were obtained from the Kaplan–Meier plotter. **G** The mRNA expression levels of SHMT1 and SHMT2 in GC cell lines were analyzed via the Cancer Cell Line Encyclopedia (CCLE) database. ***$P < 0.001$.

Table 1 | The clinicopathological features of SHMT1 in GC

Characteristics	Low expression of SHMT1	High expression of SHMT1	*P* value
Total *n*	187	188	
Pathologic T stage, *n* (%)			0.002
T1	2 (0.5%)	17 (4.6%)	
T2	37 (10.1%)	43 (11.7%)	
T3	91 (24.8%)	77 (21%)	
T4	56 (15.3%)	44 (12%)	
Pathologic N stage, *n* (%)			0.270
N0	48 (13.4%)	63 (17.6%)	
N1	47 (13.2%)	50 (14%)	
N2	43 (12%)	32 (9%)	
N3	39 (10.9%)	35 (9.8%)	
Pathologic M stage, *n* (%)			0.321
M0	164 (46.2%)	166 (46.8%)	
M1	15 (4.2%)	10 (2.8%)	
Pathologic stage, *n* (%)			0.016
Stage I	17 (4.8%)	36 (10.2%)	
Stage II	56 (15.9%)	55 (15.6%)	
Stage III	81 (23%)	69 (19.6%)	
Stage IV	24 (6.8%)	14 (4%)	
Gender, *n* (%)			0.859
Female	66 (17.6%)	68 (18.1%)	
Male	121 (32.3%)	120 (32%)	
Age, *n* (%)			0.024
<=65	93 (25.1%)	71 (19.1%)	
>65	93 (25.1%)	114 (30.7%)	
Histologic grade, *n* (%)			0.876
G1	5 (1.4%)	5 (1.4%)	
G2	65 (17.8%)	72 (19.7%)	
G3	110 (30.1%)	109 (29.8%)	
Anatomic neoplasm subdivision, *n* (%)			0.126
Antrum/Distal	76 (21.1%)	62 (17.2%)	
Cardia/Proximal	28 (7.8%)	20 (5.5%)	
Fundus/Body	53 (14.7%)	77 (21.3%)	
Gastroesophageal Junction	20 (5.5%)	21 (5.8%)	
Other	2 (0.6%)	2 (0.6%)	
Reflux history, *n* (%)			0.310
No	92 (43%)	83 (38.8%)	
Yes	17 (7.9%)	22 (10.3%)	
Antireflux treatment, *n* (%)			0.342
No	72 (40.2%)	70 (39.1%)	
Yes	22 (12.3%)	15 (8.4%)	
H pylori infection, *n* (%)			0.049
No	69 (42.3%)	76 (46.6%)	
Yes	13 (8%)	5 (3.1%)	

The cohort from TCGA database.

Table 2 | The clinicopathological features of SHMT2 in GC

Characteristics	Low expression of SHMT2	High expression of SHMT2	*P* value
Total *n*	187	188	
Pathologic T stage, *n* (%)			0.174
T1	10 (2.7%)	9 (2.5%)	
T2	37 (10.1%)	43 (11.7%)	
T3	93 (25.3%)	75 (20.4%)	
T4	42 (11.4%)	58 (15.8%)	
Pathologic N stage, *n* (%)			0.663
N0	57 (16%)	54 (15.1%)	
N1	49 (13.7%)	48 (13.4%)	
N2	32 (9%)	43 (12%)	
N3	35 (9.8%)	39 (10.9%)	
Pathologic M stage, *n* (%)			0.168
M0	166 (46.8%)	164 (46.2%)	
M1	9 (2.5%)	16 (4.5%)	
Pathologic stage, *n* (%)			0.018
Stage I	24 (6.8%)	29 (8.2%)	
Stage II	62 (17.6%)	49 (13.9%)	
Stage III	73 (20.7%)	77 (21.9%)	
Stage IV	10 (2.8%)	28 (8%)	
Gender, *n* (%)			0.092
Female	59 (15.7%)	75 (20%)	
Male	128 (34.1%)	113 (30.1%)	
Age, *n* (%)			0.429
<=65	86 (23.2%)	78 (21%)	
>65	100 (27%)	107 (28.8%)	
Histologic grade, *n* (%)			0.149
G1	8 (2.2%)	2 (0.5%)	
G2	66 (18%)	71 (19.4%)	
G3	108 (29.5%)	111 (30.3%)	
Anatomic neoplasm subdivision, *n* (%)			0.006
Antrum/Distal	71 (19.7%)	67 (18.6%)	
Cardia/Proximal	26 (7.2%)	22 (6.1%)	
Fundus/Body	50 (13.9%)	80 (22.2%)	
Gastroesophageal Junction	29 (8%)	12 (3.3%)	
Other	2 (0.6%)	2 (0.6%)	
Reflux history, *n* (%)			0.097
No	82 (38.3%)	93 (43.5%)	
Yes	24 (11.2%)	15 (7%)	
Antireflux treatment, *n* (%)			0.122
No	68 (38%)	74 (41.3%)	
Yes	23 (12.8%)	14 (7.8%)	
H pylori infection, *n* (%)			0.560
No	70 (42.9%)	75 (46%)	
Yes	10 (6.1%)	8 (4.9%)	

The cohort from TCGA database.

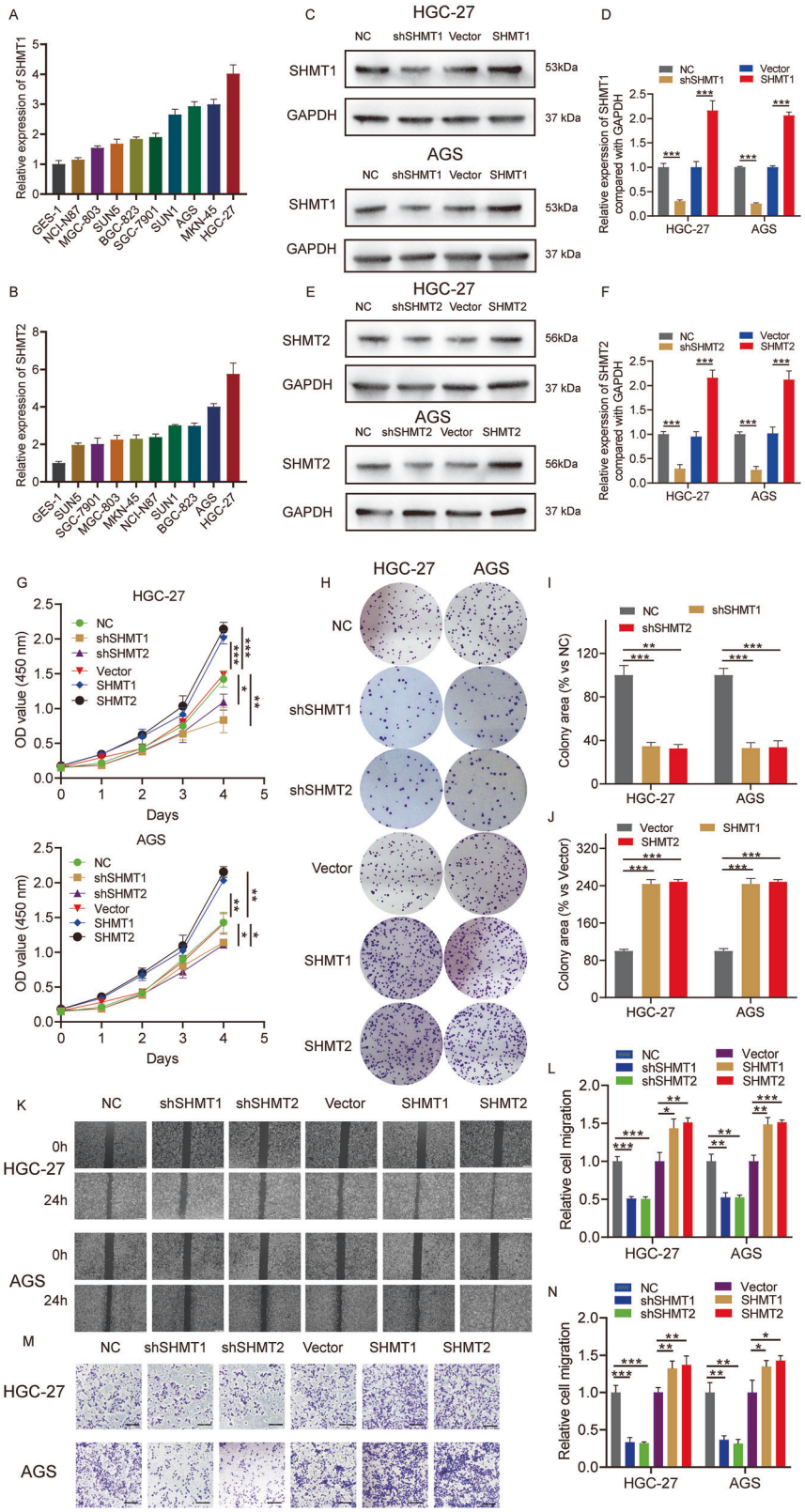

Fig. 2 | SHMT1 and SHMT2 promote the malignant progression of GC cells in vitro. A qRT-PCR assay used to detect SHMT1 expression in several GC cell lines. **B** qRT-PCR assay used to detect SHMT2 expression in several GC cell lines. **C** WB analysis showing SHMT1 expression in cells that were stably infected with lentivirus carrying NC or shSHMT1 and transfected with vector or SHMT1 overexpression plasmids. **D** Histogram reflects the expression level of SHMT1 in WB experiment. **E** WB analysis showing SHMT2 expression in cells that were stably infected with lentivirus carrying NC or shSHMT1 and transfected with vector or SHMT1 overexpression plasmids. **F** Histogram reflects the expression level of SHMT2 in WB experiment. **G** CCK-8 assays showing the proliferative capability of cells with SHMT1/2 knockdown or overexpression. **H** Colony formation assays showing the sphere formation ability of cells with SHMT1/2 knockdown or overexpression. **I**, **J** The histogram showing the colony areas in (**H**). **K** Wound healing assays showing the migration ability of cells with SHMT1/2 knockdown or overexpression. **L** The histogram showing the relative migration ratio in (**K**). **M** Transwell assays showing the migration capability of cells with SHMT1/2 knockdown or overexpression. **N** Histogram showing the relative migration ratio in (**M**). The same NC (vector)-treated control group was used for both the SHMT1 and SHMT2 experimental groups. $^{*}P < 0.05$, $^{**}P < 0.01$, $^{***}P < 0.001$.

efficiency regimen for GC, we performed a drug screening assay to determine the synergistic effect of SHIN1 with first-line chemical drugs in GC[17]. We used the SynergyFinder platform with the ZIP model to compute synergistic scores and explore combinative regimen that efficiently increased GC cell death (Fig. 3D). Notably, 5-Fu achieved the best synergistic effect on SHIN1 in GC cell lines (synergy score, 19.34 (0.95) for HGC-27 cells; 18.96 (0.62) for AGS cells) (Fig. 3E, Supplementary Fig. 2H-I). The compusyn analysis revealed that SHIN1combinative with 5-Fu improved the synergistic effects (Supplementary Fig. 2J). These results suggested that SHIN1 could be a candidate booster for 5-Fu. The IC50 of 5-Fu was 26.44 in HGC-27 cell line (Supplementary Fig. 2K). Synergy analysis revealed superior therapeutic efficacy of the 5-Fu/SHIN1 combination at 10 μM

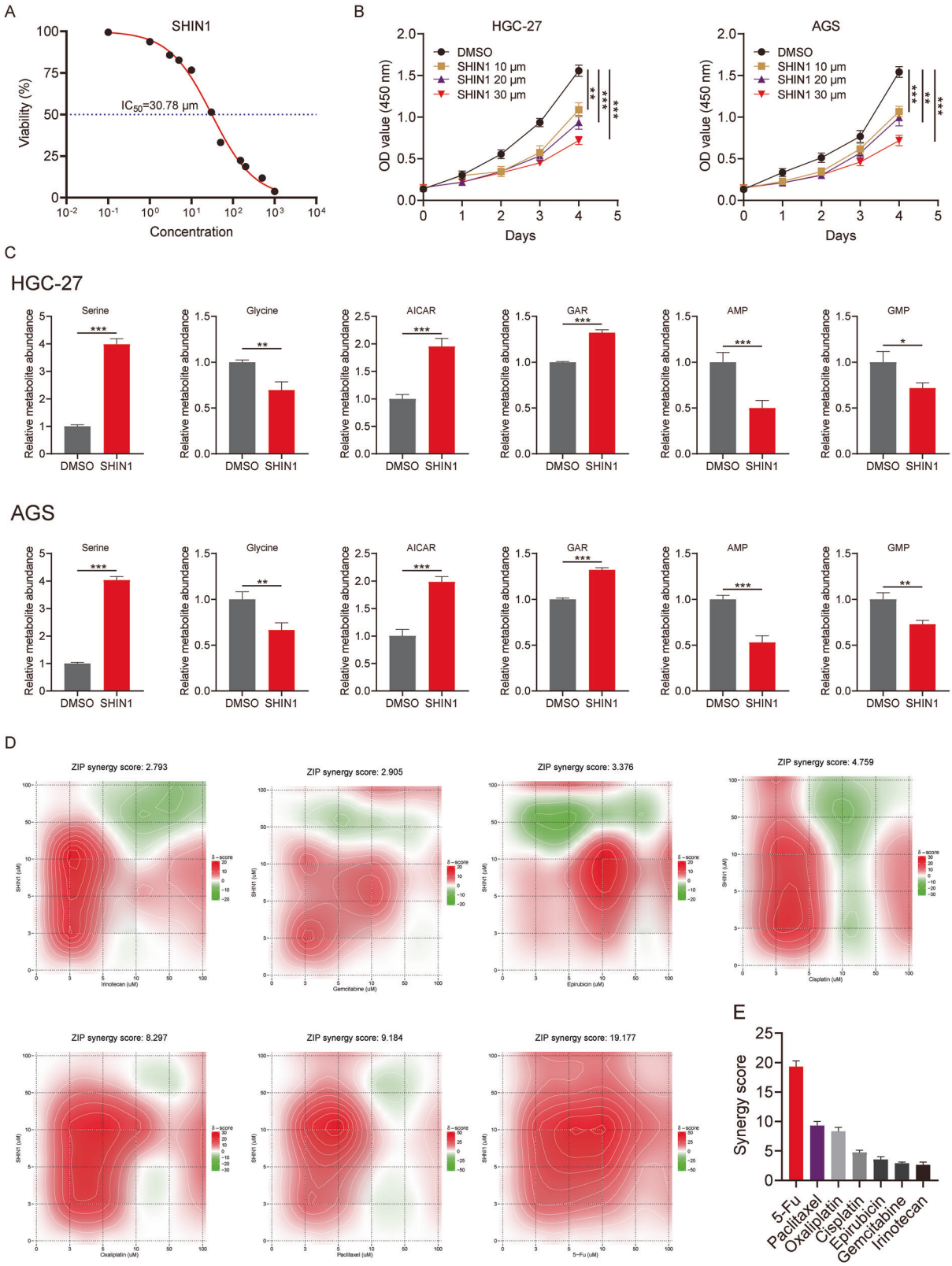

Fig. 3 | SHIN1 is a potential efficient synergistic drug for GC treatment. A The IC_{50} values generated from dose–response assays for SHIN1 in HGC-27 cells. **B** CCK-8 assays were used to detect the inhibitory effects of different doses of SHIN1 on the growth of GC cells. **C** Histograms showing the changes in metabolites correlated with one-carbon and nucleotide metabolism following treatment with SHNI1 in GC cells. Cells were treated with DMSO, SHIN1 (10 μM), 5-Fu (10 μM), or the combination of 10 μM SHIN1 with 5-Fu (10 μM). Metabolites extracted and detected using LC–MS. The raw peak areas were normalized to those of internal standards. **D** A drug screening assay was used to determine the synergistic effect of SHIN1 with first-line chemotherapy drugs for GC in HGC-27 cells. **E** The histogram showing the synergistic scores in (**D**). The SynergyFinder platform with the ZIP model was used to compute synergistic ZIP scores. $^{*}P < 0.05$, $^{**}P < 0.01$, $^{***}P < 0.001$.

concentration, which was consequently selected for subsequent experimental validation (Fig. 3D, E **and** Supplementary Fig. 2H-I).

SHIN1 significantly improved the inhibitory effects of 5-fu on gastric cancer cells

To investigate the synergistic effect of the combination of the two agents, we conducted CCK-8 assays to detect the proliferative capability of the GC cells. Compared with monotherapy, the combination of 5-fu with SHIN1 significantly inhibited the growth of GC cells (Fig. 4A, B). The MTT assay results demonstrated the toxicity and synergistic effects of SHIN1 and 5-Fu across HGC-27 and AGS cell lines, providing critical experimental evidence for optimizing chemotherapy regimens and developing novel combination strategies. The marked efficacy of combination therapy highlights its potential in overcoming single-agent resistance, particularly in tumors with heterogeneous drug sensitivity profiles. (Fig. 4C, D). Thereafter, we performed flow cytometry to verify the effect of combination treatment on apoptosis of GC cells (Fig. 4E, F). We found that SHIN1 augmented the apoptosis-inducing effect of 5-Fu, the combination treatment caused more apoptosis of GC cells. To investigate the mechanistic basis of combination therapy, we quantitatively analyzed nucleotide synthesis precursors in GC cells following combined SHIN1 and 5-Fu treatment (Fig. 4G–P). The important intermediate dUMP for synthesizing pyrimidine nucleotides accumulates due to the use of 5-Fu, leading to downstream nucleotide synthesis disorders[18]. The combined use of SHIN1 further amplifies this effect (Fig. 4G, L). Besides, pyrimidine nucleotides also significantly decreased in the combination group (Fig. 4H–K, M–P). Overall, these findings indicate that SHIN1 imporve the therapeutic effect of 5-Fu by interfering nucleotide synthesis of GC cells, but the potential underlying molecular mechanism deserves further elucidation. We hope that the highly efficient combination of SHIN1 with 5-Fu could lead to the selection of novel therapeutic agents for GC patients.

SHIN1 combination with 5-Fu triggered multiple inhibitory pathways in gastric cancer

To further explore the mechanism underlying the synergistic effect of the combination of SHIN1 with 5-Fu, we evaluated the transcriptomic profiles of HGC-27 cells under four different treatment regimens at 48 h. The combination of SHIN1 and 5-Fu, compared with that of either monotherapy, induced specific alterations in the transcriptomic level (Fig. 5A–C). Gene Ontology (GO) and Kyoto Encyclopedia of Genes and Genomes (KEGG) enrichment analyses were conducted to identify differentially expressed genes and associated pathways (Fig. 5D, E).

The analysis revealed that genes involved in the cell cycle were the most significantly changed genes in both analyses (Fig. 5D). Cellular senescence refers to an irreversible cell cycle arrest induced by factors such as oncogene activation and DNA damage (Fig. 5E). The genes involved in cell senescence and DNA damage were affected by the combination of SHIN1 and 5-Fu. In addition, the P53 signaling pathway, an important cancer-inhibiting pathway, was also activated by the combination treatment of SHIN1 with 5-Fu ($P = 0.02$, NES = 1.349, FDR q-value = 0.145, Fig. 5F). We constructed a heatmap to show the differentially expressed genes related to the cell cycle, cell senescence and the P53 pathway based on the GO and KEGG analyses (Fig. 5G). The P21, identified as the most significant in the combination treatment, plays a crucial role in promoting cell cycle arrest and cellular senescence (Fig. 5H). Consistent with the findings of previous studies, the cell cycle-related genes CDK4/6 were inhibited by the combination treatment of SHIN1 and 5-Fu (Fig. 5G). Growth arrest and DNA damage protein 45 A (GADD45A) and cyclin-dependent kinase inhibitor 1 A (CDKN1A, P21) were triggered significantly by the combination treatment (Fig. 5G). SHIN1 and 5-fu may have different effects on the P53 signaling pathway at the transcriptomic level due to differences in their mechanisms of action, but their synergistic effect can efficiently activate the P53 signaling pathway (Fig. 5G). These findings suggest that cell cycle arrest and cellular senescence may be mediated by the P53 signaling pathway, and its potential molecular mechanisms deserve further investigation and validation. The combination therapy breaks the genetic balance of malignant proliferation in GC cells. We explored the association between SHMT isoforms expression and cell cycle regulatory proteins using Spearman correlation analysis. Notably, the two SHMT isoforms demonstrated divergent expression profiles and differential correlation trends across specific cell cycle-related genes, with distinct coefficient values distinguishing their associations (Supplementary Fig. 3A–J). Based on the above research, further testing is needed to investigate the changes in cell cycle related proteins after inhibiting the two subtypes of SHMT, as well as their role in combination drug therapy.

The combination treatment induces DNA damage and cellular senescence through the regulation of the P53 signaling pathway

Flow cytometric analysis of the cell cycle was used to compare the cell populations in the different treatment groups. GC cells treated with DMSO, 5-Fu, SHIN1, or SHIN1 + 5-Fu exhibited differences in the three phases of the cell cycle. The combination treatment significantly increased the proportion of GC cells in G1 phase arrest, whereas treatment with SHIN1 or 5-Fu alone caused a moderate G1 phase arrest (Fig. 6A–D). Notably, the SHIN1 treatment sensitized cells to the cell cycle arrest induced by 5-Fu. The phosphorylated form of histone H2AX (γ-H2AX) is a commonly utilized biomarker for DNA damage[19]. We used an IF assay to measure the expression of γ-H2AX in the four treatment groups (Fig. 6E, F). We noted that combination treatment of SHIN1 with 5-fu in GC cells triggered higher expression of γ-H2AX than monotherapy with SHIN1 or 5-Fu. Similarly, a biomarker of cellular senescence, senescence-associated beta-galactosidase (SA-beta-gal), was detected in our treatment groups[20]. There were significantly more stained cells in the combination treatment group (Fig. 6G, H). These findings validate that the combination treatment caused further DNA structural damage in GC cells.

We used the WB assay to detect P53 signaling pathway-related proteins in experimental groups (Fig. 6I, J). P53, as the main initiating factor of this signaling pathway, was significantly activated in the combination therapy group. The inconsistent expression of P53 in two cell lines may be related to the presence of wild-type or mutant status in cell lines[21,22]. However, the expression of P53 was significantly increased in the combination therapy groups. It is speculated that this phenomenon may be due to SHIN1 and 5-Fu activating P53 through distinct molecular mechanisms, with the combination therapy further enhancing P53 expression levels via synergistic effects. CDKN1A (P21) and GADD45A, which are tumor suppressive factors could induce cell cycle arrest and cell senescence, were significantly upregulated in the combination groups compared to those in the SHIN1 or 5-Fu monotherapy groups[23,24]. CDK4/6 are important cell cycle-dependent proteins that promote GC progression[25]. WB analysis also revealed that the combination of SHIN1 with 5-Fu significantly inhibited the expression of CDK4 and CDK6 (Fig. 6I, J).

The activation of the P53 signaling pathway in GC cells was further evaluated under SHIN1 and 5-Fu treatments. IF assay revealed enhanced nuclear accumulation of P53 in cells treated with SHIN1 alone or combined with 5-Fu, compared to DMSO group (Supplementary Fig. 4A-B). Quantitative fluorescence intensity confirmed that the combination treatment significantly induced P53 activation in both cell lines (Supplementary Fig. 4C-D). We further investigate the effect of P53 inhibitors on combination therapy (Supplementary Fig. 4E-N). The gene expression profiling demonstrated that the SHIN1/5-Fu combination synergistically induced the expression of P21 and GADD45A (Supplementary Fig. 4F, G, K, L) while suppressing cell cycle drivers CDK6 and CDK4 (Supplementary Fig. 4H, I, M, N)—effects that were reversed by the P53 inhibitor PFT-α. These results verified the combination-induced transcriptomic changes in GC cells in vitro. The specific mechanism of activating P53 through combination therapy deserves further exploration.

The combination of 5-Fu and SHIN1 has potent antitumour effects in vivo

To evaluate the therapeutic efficacy of SHIN1 and 5-Fu combination, we established a cell-derived xenograft (CDX) model using the HGC27 cell line.

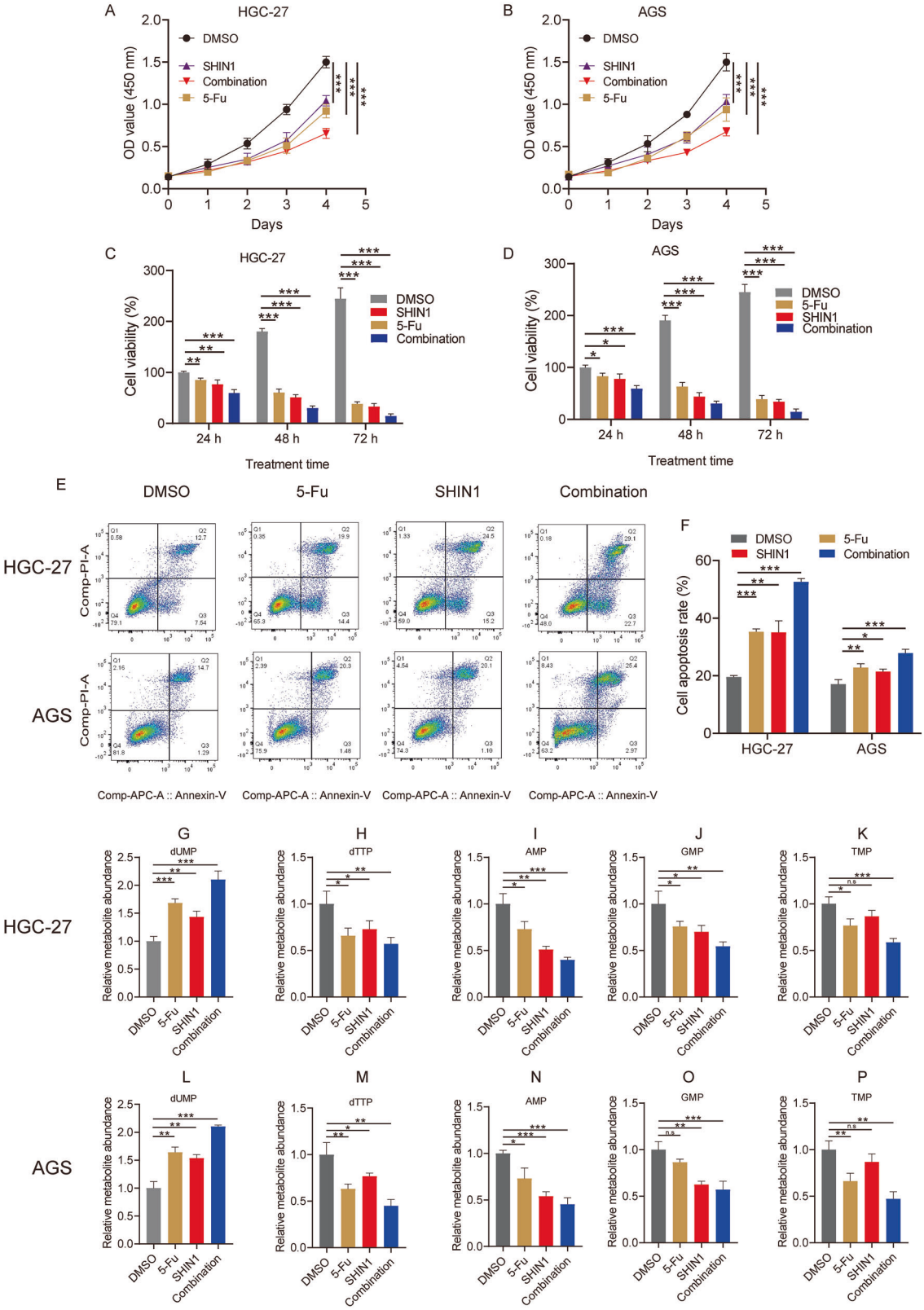

Fig. 4 | The combination of 5-Fu with SHIN1 had favorable antitumour effects on GC. A CCK-8 assays showing the growth inhibitory effects of monotherapy or combination therapy on HGC-27 cells. **B** CCK-8 assays showing the growth inhibitory effects of monotherapy or combination therapy on AGS cells. **C** MTT assays showing the inhibitory effects of monotherapy or combination therapy on cell proliferation in HGC-27 cells. **D** MTT assays showing the inhibitory effects of monotherapy or combination therapy on cell proliferation in AGS cells. **E**, **F** Flow cytometry assays showing the apoptotic effects of monotherapy or combination therapy on GC cells. **G**–**P** Histograms showing changes in metabolites correlated with nucleotide metabolism following monotherapy or combination therapy. Cells were treated with DMSO; SHIIN1: 10 μM; 5-Fu: 10 μM; or the combination of 10 μM SHIIN1 with 10 μM 5-Fu. Metabolites extracted and detected using LC–MS or corresponding reagent kit. $^{*}P < 0.05$, $^{**}P < 0.01$, $^{***}P < 0.001$.

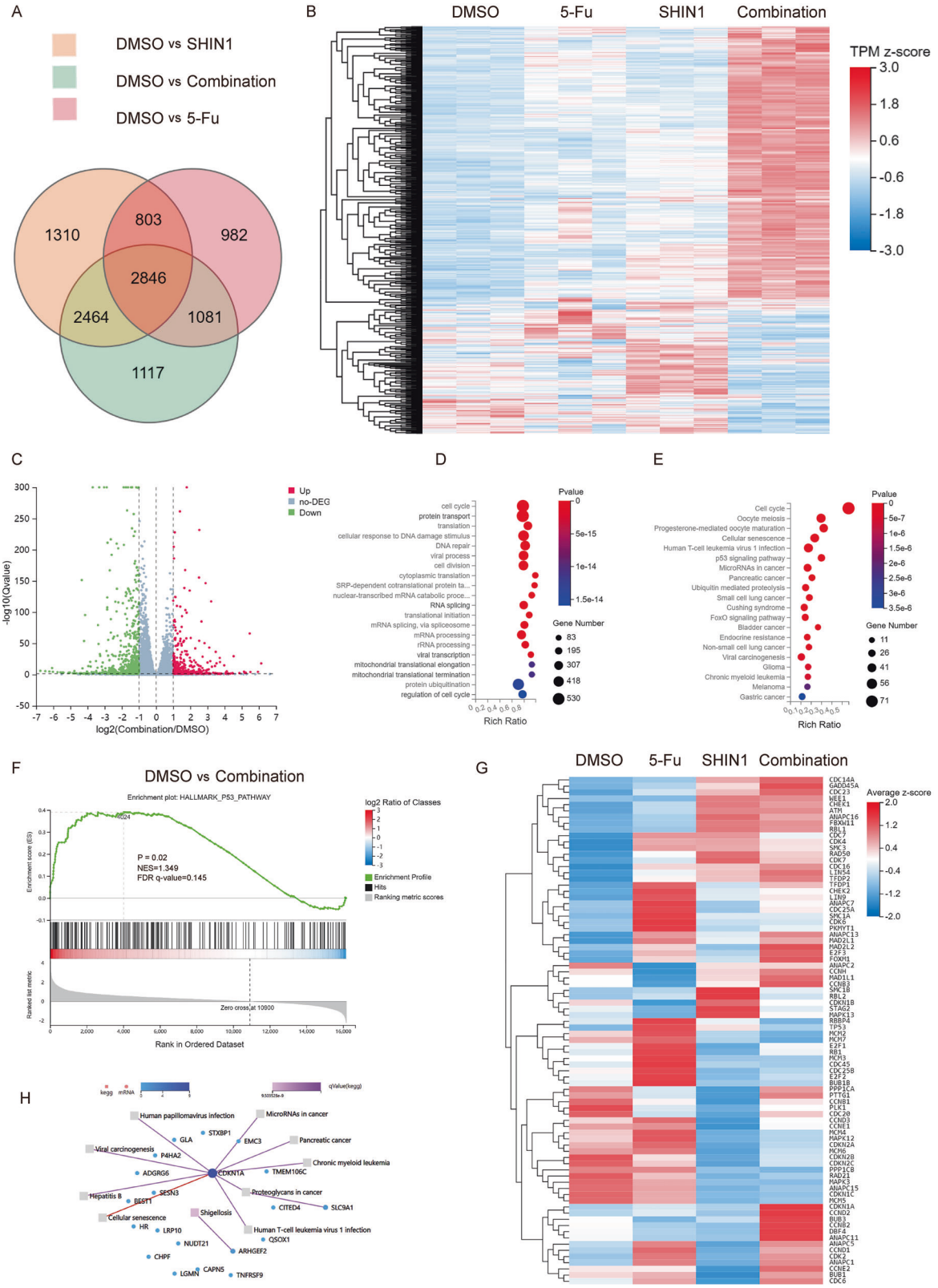

Fig. 5 | The molecular mechanism of the interaction between 5-Fu and SHIN1 in GC cell lines revealed by RNA-seq. A The Venn diagram shows differentially expressed genes among the monotherapy and combination therapy groups. **B** Heatmap of differentially expressed genes in HGC-27 cells after different treatments. **C** The volcano plot to show the differential genes between combination treatment and control group. **D** GO enrichment analysis of the differentially expressed genes. **E** KEGG enrichment analysis of differentially expressed genes involved in the cell cycle between DMSO and Combination groups. **F** GSEA plots of P53 signaling pathway components in the different treatment groups. **G** Heatmap of differentially expressed genes among the cell cycle, cell senescence and P53 signaling pathways based on GO and KEGG analyses. **H** The top 20 genes with the most significant changes in combination treatment group and KEGG enrichment analyses for CDKN1A.

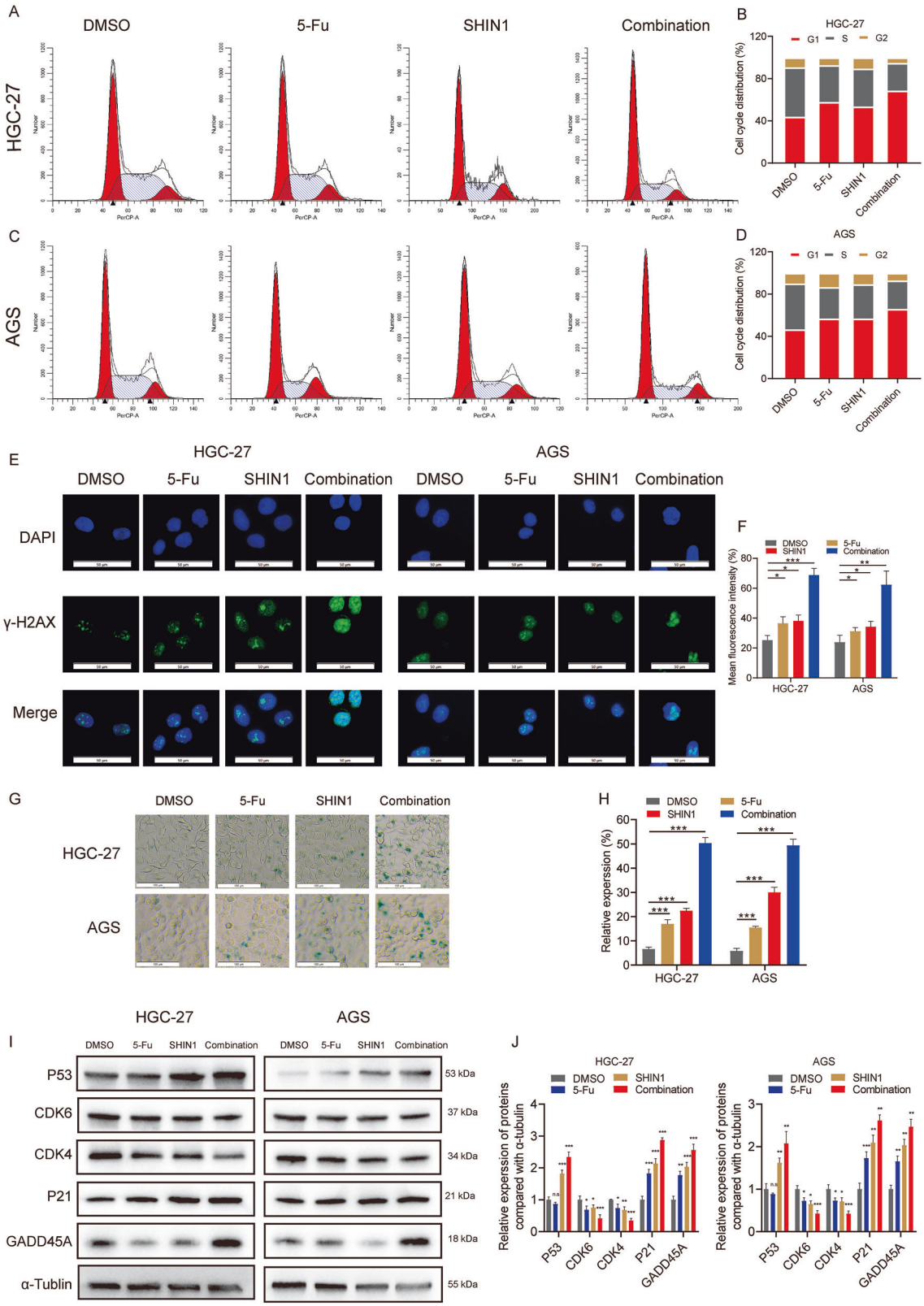

Fig. 6 | The combination of SHIN1 and 5-Fu specifically induced cell cycle arrest, DNA damage and cell senescence in vitro. A Representative cell cycle plots of HGC-27 cells treated with DMSO; SHIIN1: 10 μM; 5-Fu: 10 μM; and the combination of 10 μM SHIIN1 with 10 μM 5-Fu for 48 h. **B** Representative histograms of the ratios of cells in the G1, S, and G2 phases are shown. **C** Representative cell cycle plots of AGS cells treated with DMSO; SHIIN1: 10 μM; 5-Fu: 10 μM; and the combination of 10 μM SHIIN1 with 10 μM 5-Fu for 48 h. **D** Representative histograms of the ratios of cells in the G1, S, and G2 phases are shown. **E** Representative photos of γ-H2AX (a biomarker of DNA damage) stained by IF in two GC cell lines. **F** Histogram of the fluorescence intensity in (**E**). **G** Representative images of SA-beta-gal (a biomarker of cell senescence) staining in two GC cell lines. **H** Histogram of the positive cells in (**G**). **I** WB assays were used to detect the expression of cell cycle-related proteins. **J** Histogram to show the relative expression of cell cycle-related proteins. $^{*}P < 0.05$, $^{**}P < 0.01$, $^{***}P < 0.001$.

The combination of SHIN1 and 5-Fu, compared to monotherapy, significantly limited tumor growth in the HGC-27 xenograft model (Fig. 7A, B). Similarly, the tumor weight was also obviously reduced by the combination of 5-Fu and SHIN1 (Fig. 7C, D). Moreover, all mice in the experiments tolerated the treatment well during the dosing process. These results illustrated the efficient inhibitory effect of the combination of SHIN1 with 5-Fu on tumor growth in vivo. We further used an IHC assay to detect the expression of cell cycle-related proteins in tumor-derived slices (Fig. 7E). Pathological analysis revealed that the combination of SHIN1 with 5-Fu apparently inhibited the activity of CDK4/6 and promoted the expression of P53, P21 and GADD45A in tumors (Fig. 7E). These results support the conclusion that combination therapy induces cell cycle arrest and subsequently inhibits tumor proliferation.

SHIN1 alleviates 5-Fu resistance and improves its inhibitory effects on GC

To assess the resistance of GC cells to 5-Fu, xenograft-derived cells were used to establish a 5-Fu-resistant GC cell line[26]. We generated 5-Fu-sensitive cell lines (HGC-27/S) and 5-Fu-resistant cell lines (HGC-27/R) by primary culture of 5-Fu-sensitive and 5-Fu-resistant tumor samples, respectively (Fig. 8A). We further verified the reactivity of these cells to 5-Fu by proliferation assays. According to the results, the IC50 values of 5-Fu in resistant cells were significantly higher than those in sensitive cells (Fig. 8B). CCK-8 and colony formation assays were subsequently used to assess the proliferative capacity of the two cell lines (Fig. 8C–E). As a result, the resistant cells had greater proliferative potential; however, SHIN1 alleviated 5-Fu resistance and augmented the growth inhibitory effects of 5-Fu on GC. We further performed a flow cytometry assay to measure the cell apoptosis rate in both 5-Fu-resistant and 5-Fu-sensitive cells (Fig. 8F, G). The results revealed that SHIN1 promoted the therapeutic efficacy of 5-Fu. We further measured SHMT expression levels in HGC-27 cells and tumor tissues categorized into 5-Fu-sensitive and -resistant subgroups (Fig. 8H, I). These findings demonstrate that both SHMT1 and SHMT2 are significantly upregulated in 5-Fu-resistant cells, providing critical evidence for the involvement of SHMT isoforms in mediating 5-Fu resistance mechanisms in GC.

Currently, the clinical treatment of advanced GC is not promising. Elucidating the molecular mechanisms of malignant progression and exploring new diagnostic and therapeutic targets are urgently needed. Previous studies have revealed the significance of the glycine-serine metabolism pathway in tumor progression and metastasis[7,27]. This pathway may be crucial in the malignant progression of GC.

SHMT promotes tumor progression through multiple mechanisms. Thanh H et al. reported that SHMT2 promotes the growth of alveolar rhabdomyosarcoma (RMS) cells and that its targeted inhibition could be effective for treatment[12]. Gregory S et al. found a positive correlation between SHMT activity and proliferation in patients with diffuse large B-cell lymphoma (DLBCL)[28]. Yun Zhang et al. revealed that SHMT2 promotes the growth of bladder cancer through multiple internal signaling pathways and inhibits mitochondria-mediated cell apoptosis[29]. Knockdown of SHMT1 induces apoptosis in lung cancer cells through uracil misincorporation[30]. However, SHMT is an important hub between nucleotide synthesis and glycine metabolism, and the underlying mechanism in GC has not been fully elucidated. Several previous studies reported that SHMT is involved in the malignant biological behaviors of GC[11,31]. These studies suggest that elevated SHMT2 expression is associated with tumor progression and poor prognosis in GC patients[31]. In GC cells with low Drosha expression, miR-6778-5p upregulates SHMT1, driving compensatory activation of cytoplasmic carbon metabolism, which is critical for maintaining gastric cancer stem cell (GCSC) stemness[11]. These results showed the potential value of SHMT in the development of targeted drugs for GC treatment.

SHIN1, a targeted inhibitor of SHMT1 and SHMT2, has been explored for the treatment of various tumors. Gregory et al. reported that the glycine deficiency caused by SHIN1 is a potential mechanism that hinders the growth of DLBCL cells[28]. SHIN1 inhibited these enzymes in the one-carbon folate pathway and induced cell cycle arrest in acute lymphoblastic leukemia (ALL) cells[18]. Suppression of glycogen synthase kinase 3 (GSK3) enhances serine/one-carbon metabolism and exerts a significant synergistic effect with SHIN1 in inhibiting lung cancer cell proliferation[13]. The inhibition of SHMT1 significantly reduced the formation of GCSC spheres and increased the sensitivity of GC cells to 5-Fu treatment[11]. These studies led us to consider whether SHIN1 could be applied in the treatment of GC. We explored the inhibitory effect of SHIN1 on GC cells and further screened its potential synergistic effects in this study.

Currently, chemotherapy is considered the most common treatment for advanced GC. 5-Fu is a common antimetabolite of uracil and has been widely used to treat GC[32]. 5-Fu is metabolized in the body to produce fluorouracil deoxyribonucleotides and interfere with tumor cell DNA synthesis, thus exerting antitumour effects. It can also be converted into fluorouracil nucleoside and incorporated into RNA to influence protein synthesis. The first-line treatment methods for GC include 5-Fu and a platinum-based agent, namely, XELOX (oxaliolatin+capecitabine), SOX (S-1+oxaliplatin) and FOLFOX (leucovorin+5-Fu+oxaliplatin)[17]. However, chemoresistance has limited therapeutic efficacy of those dosage regimens[33]. Hence, new therapeutic options are urgently needed for the treatment of GC. Based on the cancer-promoting mechanism of SHMT, its inhibitor SHIN1 was utilized in the treatment of GC in a preclinical study. The combination treatment induced cell senescence and DNA damage in GC cells. We found evident synergistic effects of the combination of 5-Fu with SHIN1 in in vivo and in vitro GC models. Assays finished on cell lines and mice supported the transcriptomic results that cell cycle arrest occurred under the combination treatment of 5-Fu and SHIN1. We also found that SHIN1 alleviated 5-fu resistance and augmented its anticancer effects on GC. These findings align with previous studies showing that SHIN1 enhances the sensitivity of GC cells to 5-Fu treatment.

The regulatory function of P53 in cell cycle control serves as a pivotal biological hallmark in the pathogenesis and progression of GC[34]. This study noticed different expression of P53 protein in HGC-27 and AGS cell lines. However, combination treatment with 5-Fu and SHIN1 induced significant P53 upregulation in both cell types, implying distinct intrinsic P53 genetic profiles[21,22,35]. Mechanistically, 5-Fu disrupts DNA replication by inhibiting thymidylate synthase (TS), whereas SHIN1 triggers metabolic stress via blockade of the serine-glycine biosynthesis pathway, ultimately depleting nucleotide precursors and inducing DNA damage. The therapeutic synergy likely stems from complementary molecular actions: 5-Fu targets enzymatic inhibition in DNA synthesis, while SHIN1 remodels the tumor metabolic niche to amplify genomic instability[14,36]. This multi-modal intervention not only reactivates the functional P53 signaling cascade but also overcomes intercellular genetic heterogeneity, underscoring its efficacy in diverse cancer models with variable P53 status.

Previous studies have provided evidence that cell cycle kinases are promising therapeutic candidates for patients resistant to first-line therapies[25,37]. We found that CDK4 and CDK6 were significantly inhibited by the combination treatment of SHIN1 and 5-Fu. In addition, the tumor suppressive factors CDKN1A and GADD45A were triggered by the combination treatment. Several CDK4/CDK6 inhibitors have been evaluated in clinical trials for GC treatment, either as monotherapies or in combination with other drugs (NCT03891784, NCT03480256, and NCT02378389)[38]. Some studies have shown that treatment with a single inhibitor has lower medicinal efficacy. Moreover, the combination of these agents with other drugs that may augment the treatment efficacy is more effective[25,26,39]. Thus, candidate drugs that combine with SHIN1 to enhance the effectiveness of GC treatment need to be explored. Our results provide important evidence that the combination of SHIN1 with 5-Fu efficiently promotes cell cycle arrest to inhibit GC.

Overall, the combination therapy integrates the anticancer mechanisms of both SHIN1 and 5-Fu, leading to cell cycle arrest and GC cell growth inhibition. 5-Fu interferes with the synthesis of pyrimidine nucleotides, and SHIN1 reduces the supply of glycine and one carbon unit, which serve as necessary materials for the synthesis of purine nucleotides[18,40].

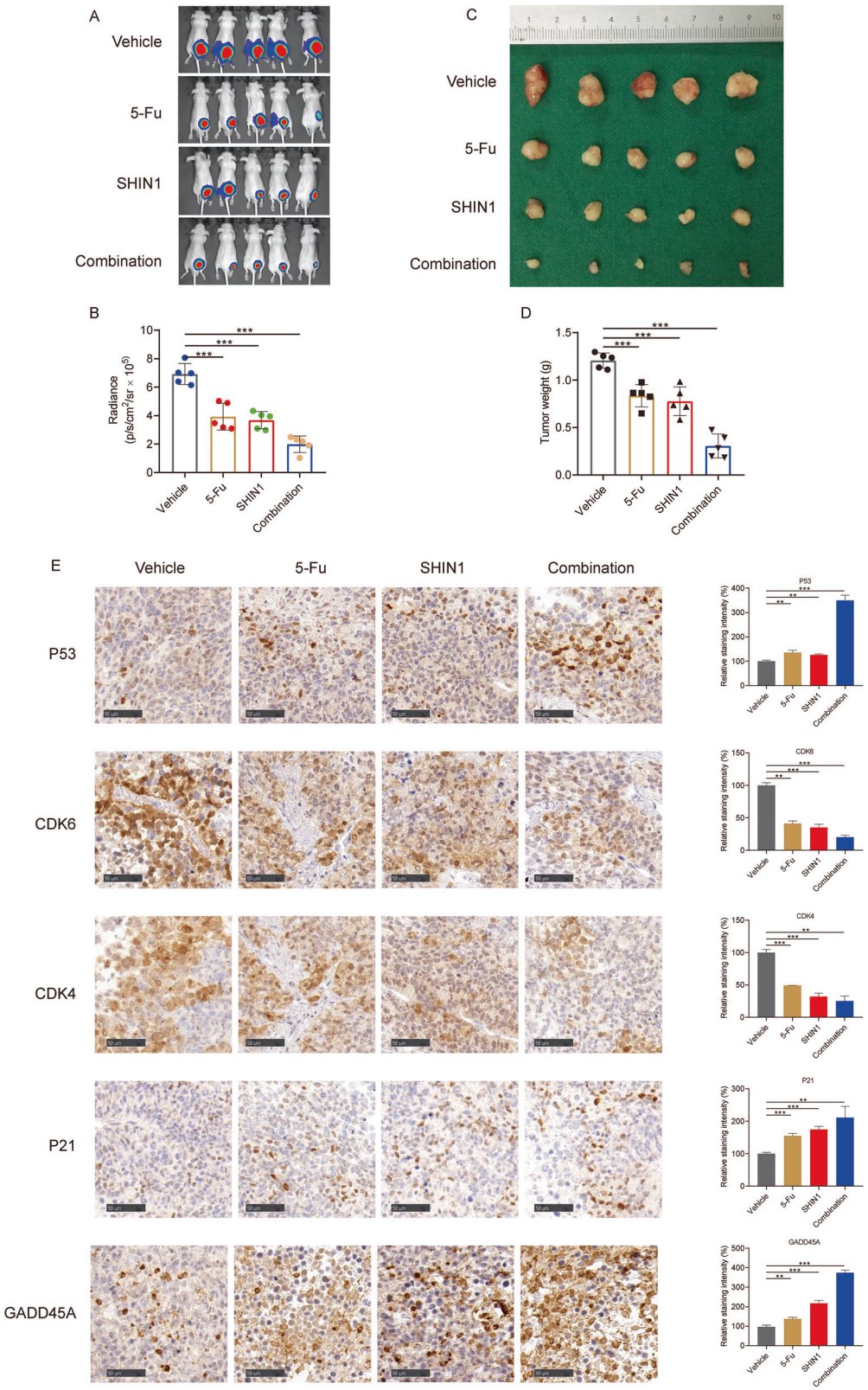

Fig. 7 | The combination of SHIN1 with 5-Fu inhibited tumor growth in vivo through inducing cell cycle arrest. A Luminescent intensities of subcutaneous tumors in nude mice treated with vehicle, 5-Fu, SHIN1 or the combination therapy. **B** Histogram showing the relative luminescence intensities in mice treated with different methods. **C** Tumors derived from nude mice that were treated with different methods. **D** Histogram showing the relative tumor weights of mice treated with different methods. **E** Representative graphs of IHC staining for several cell cycle-related proteins and corresponding histograms showing the relative staining intensity. Tumor-bearing mice received vehicle, 5–Fu (10 mg kg^{-1} body weight), SHIN1 (100 mg kg^{-1} body weight) or the combination treatment (10 mg kg^{-1} 5-Fu and 100 mg kg^{-1} SHIN1) by intraperitoneal injection. The dose of the injection was referenced previous studies and validated by a series of pre-experiments. $^{*}P < 0.05$, $^{**}P < 0.01$, $^{***}P < 0.001$.

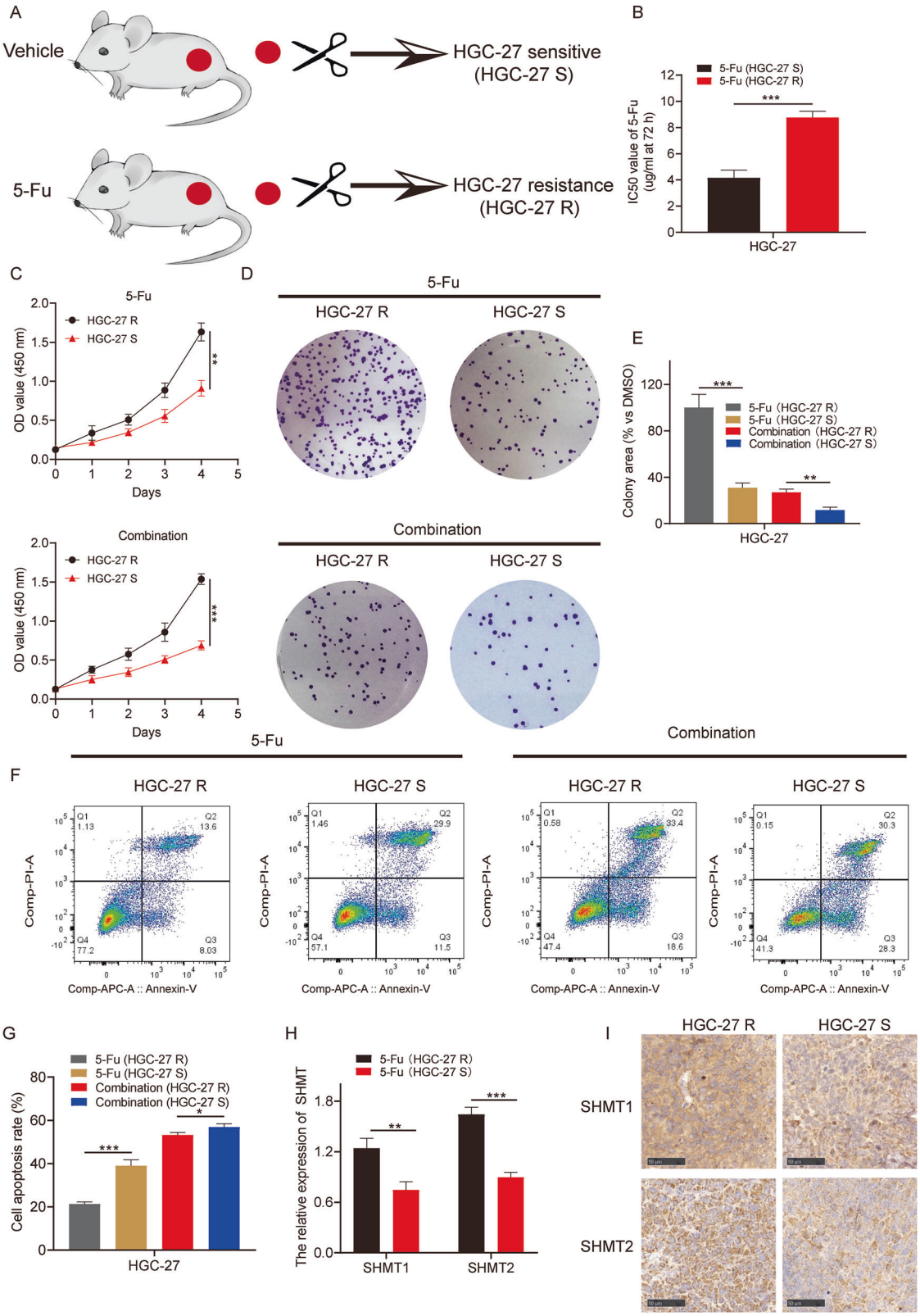

Fig. 8 | SHIN1 alleviated 5-Fu resistance in GC cells. A A sketch of the 5-Fu-resistant cell line construction. **B** The IC_{50} values of 5-Fu were detected in 5-Fu-sensitive (5-Fu S) and 5-Fu-resistant (5-Fu R) cells through CCK-8 assays. **C** Cell viability assays were used to assess the proliferative ability of both 5-Fu S and 5-Fu R cells treated with DMSO, 5-Fu (10 μM), SHIN1 (10 μM) or the combination of both 5-Fu (10 μM) and SHIN1 (10 μM). **D** Colony formation assays were applied to evaluate the proliferative ability of both 5-Fu S and 5-Fu R cells, which were treated with DMSO, 5-Fu (10 μM), SHIN1 (10 μM) or the combination of both 5-Fu (10 μM) and SHIN1 (10 μM). **E** The histogram showing the colony areas in (**D**). **F** Flow cytometry was used to measure the cell apoptosis rate of 5-Fu S and 5-Fu R cells; which were treated with DMSO, 5-Fu (10 μM), SHIN1 (10 μM) or the combination of both 5-Fu (10 μM) and SHIN1 (10 μM) for 48 h. **G** Histogram showing the apoptosis rate in (**F**). **H** The relative expression of SHMT in HGC-27 cells, which resistance or sensitive to 5-Fu (qRT-PCR). **I** The IHC staining of SHMT in subcutaneous tumors. $^{*}P < 0.05$, $^{**}P < 0.01$, $^{***}P < 0.001$.

Transcriptomic analysis revealed that SHIN1 amplified the effects of 5-Fu on cell cycle arrest, DNA damage and cell senescence. These results were validated by in vivo and in vitro assays and will provide an efficient preclinical model for the treatment of GC.

This study has several limitations. First, we explored only the malignant progressive mechanisms of SHMT in cell lines, whereas the comprehensive regulatory landscapes of SHMT were not identified. Second, the cytotoxic effects of the therapeutic model on normal human cells were not clarified. Third, future studies should elucidate the mechanism of cell cycle arrest and chemoresistance associated with combination treatment. Fourth, The specific molecular mechanisms underlying the gain-of-function of P53 mediated by 5-Fu and SHIN1 remain to be elucidated.

Small molecule inhibitors are promising targeted treatments for tumors and are being investigated for their efficacy in treating GC. SHMT is frequently altered in GC, and its targeted inhibitor SHIN1 has shown efficient therapeutic efficacy in numerous tumors. Our results confirmed that SHMT1 and SHMT2 promoted the malignant progression of GC and were significantly elevated in 5-Fu-resistant GC cells. We also revealed that SHIN1 was the effective synergist for 5-Fu treatment. Transcriptomic analysis revealed that SHIN1 synergizes with 5-Fu to augment DNA damage, induce cell senescence and promote cell cycle arrest through regulating P53 signaling pathway. This multi-modal intervention not only reactivates the functional P53 signaling cascade but also overcomes intercellular genetic heterogeneity. We validated the efficacy of combination 5-Fu with SHIN1 using in vitro assays and in vivo CDX model. This study offers experimental evidence and a detailed mechanistic analysis, proposing a novel combination therapy for further clinical evaluation in GC.

Methods

Cell culture

The mycoplasma-free cell lines used in this study were sourced from the Cell Bank of the Chinese Academy of Sciences (Shanghai, China). HGC-27 cells stably harboring luciferase were previously established and stored at our center. The cells were cultured in Dulbecco's modified Eagle's medium (Gibco, NY, USA) supplemented with 1% penicillin-streptomycin solution (100×) (Corning, CA, USA) and 10% fetal bovine serum (FBS; Solarbio, Beijing, China). The cells were cultured at 37 °C in the presence of 5% CO2.

Quantitative real-time PCR (qRT–PCR)

Total RNA was extracted from the treated cells with TRIzol reagent (Invitrogen). An ExScript RT–PCR kit (TaKaRa, Kyoto, Japan) was performed with first-strand cDNA. RT-PCR was performed using SYBR Green PCR reagent (TaKaRa). GAPDH was used as an internal control for comparisons. The relative expression of the genes was normalized to that of the corresponding control and was subsequently calculated by the $2^{-\Delta\Delta Ct}$ method. The primers used for the targeted genes are listed in Supplementary Table 1.

Cell transfection and lentiviral infection

The overexpression plasmids targeted short hairpin RNAs (shRNAs) were obtained from JTS Scientific (Wuhan, China). The cells were transfected according to the Lipofectamine 3000 (Invitrogen, CA, USA) protocol. A lentiviral packaging kit (Yeasen, Shanghai, China) and the HEK-293T cell line were used in this study. AGS and HGC-27 cells were cultured with lentivirus for 48 h. The treated cells were screened with 1 μg/mL puromycin for 10 days. The targeted sequences of the shRNAs are listed in Supplementary Table 2.

Dose-dependent assay

A moderate density of GC cells was plated in a 96-well plate. After post-adherence, the culture medium was changed for drug treatment. The luminescent signal was detected with CellTiter-Glo (CTG). After 72 h of drug treatment, a SYNERGY H1 microplate reader (BioTek, VT, USA) was used to measure the viability of the GC cells. Ten consecutive doses of SHIN1 and three biological replicate groups were used in this study. Prism version 8.0 (Prism Software Corporation, CA, USA) was used to construct a sensitivity curve and calculate the 50% inhibition concentration (IC50).

Drug synergy analysis

A moderate density of GC cells was plated in 384-well plates. After post-adherence, the culture medium was changed for drug treatment. The luminescent signal was detected with a CellTiter-Glo (CTG) system. The appropriate dose of SHIN1 combined with 5-Fu was explored for the treatment of GC cells. After 72 h of drug exposure, a SYNERGY H1 microplate reader (BioTek, VT, USA) was used to measure the viability of the GC cells. Synergistic analysis with the Zero-Inflated Poisson (ZIP) model was performed, and the results were visualized via the SynergyFinder platform (RRID:SCR_019318). We tested 5 doses of SHIN1 that were combined with five concentrations of chemical drugs (24 dose combinations) for GC in triplicate. The potential synergistic effect was analyzed using the software CompuSyn (Cambridge, UK). The drugs used in the study are listed in Supplementary Table 3.

Western blot (WB) assay

The collected cells were treated with radioimmunoprecipitation (RIPA) buffer (Solarbio, Beijing, China). A BCA protein assay kit (Thermo Fisher, Shanghai, China) was used for total protein quantification. The protein extracts were distributed via 10% sodium dodecyl sulfate–polyacrylamide gel electrophoresis (10% SDS-PAGE). The proteins on the gels were subsequently transferred onto polyvinylidene fluoride (PVDF) membranes (Millipore, MA, USA). The treated membranes were blocked with 5% bovine serum albumin (BSA) for 1 h at room temperature. The corresponding primary antibodies were incubated overnight at 4 °C. Species-matched secondary antibodies were incubated for 1.5 h at room temperature. During all the intervals between the transitional processes, the membranes were washed with 1× Tris-buffered saline-Tween (TBST) for 10 min (three times). α-Tubulin and GAPDH were used as the internal control for comparison. The ECL luminescent chromogenic solution (Beyotime, Shanghai, China) was used to visualize the protein bands. The antibodies used in the study are listed in Supplementary Table 4.

Cell counting Kit-8 (CCK-8) assay

Cells were plated at an appropriate density (3×10^3) in 96-well plates. After the cells had adhered, the medium was replaced with FBS-free medium containing 10% CCK-8 solution (Abmole, Shanghai, China). The treated cells were cultured in a 37 °C incubator for 1.5 h, after which the absorbance at 450 nm was detected. The viability of the cells was measured at the indicated times, and Prism was used to construct a proliferative curve.

MTT assay

Cell viability and cytotoxicity were assessed using the MTT assay. Briefly, GC cells were seeded in 96-well plates at a density of 5×10^3 cells/well in 100 μL medium supplemented with 10% fetal bovine serum (FBS) and incubated for 24 h at 37 °C under 5% CO_2 to ensure adhesion. Test compounds or vehicle controls were added to triplicate wells and incubated for 24–72 h. After treatment, 20 μL of MTT solution (5 mg/mL in PBS) was added to each well (final concentration: 0.5 mg/mL), followed by 4 h incubation to allow viable cells to reduce MTT to formazan crystals. The supernatant was aspirated, and formazan crystals were solubilized in 150 μL DMSO with 10 min agitation in the dark. Absorbance was measured at 570 nm using a microplate reader. Cell viability was calculated by normalizing the absorbance of treated cells to untreated controls and blank wells.

Colony formation assay

The appropriate density of cells (1×10^3) was plated in 6-well plates. After the cells had adhered, the medium was replaced with drug-treated medium, and the cells were cultivated in an incubator. The corresponding media were changed every three days. After 14 days, the treated cells were washed with 1× PBS and then fixed with 4% paraformaldehyde (Sigma-Aldrich) for 20 min at room temperature. The fixed cells were washed twice with 1× PBS

and subsequently stained with crystal violet (Sigma) for 30 min at room temperature. The cells were photographed after washing with distilled water three times.

Wound healing assay

The appropriate density of cells was plated in 6-well plates. After the cells had adhered, the wounds were scratched with 200 μL pipette tips. The scratched cell monolayers were photographed after washing with PBS three times. The treated cells were cultured in a 37 °C incubator for 24 h. The wound areas were assessed for further comparison of the cell migration rate at 0 h and 24 h.

Transwell assay

Transwell assay was conducted using 24-well Transwell inserts (Corning, NY, USA) with 8-μm pores. A total of 3×10^4 cells were seeded in the upper chamber with serum-free medium and 600 μL of medium containing 20% FBS was added to the lower chamber as the chemoattractant for GC cells. After 24 h, 4% paraformaldehyde was used to fix cells at room temperature for 15 min. Cells were subsequently stained with 0.1% crystal violet for 15 min at room temperature. Images of migrative cells in the lower chamber were acquired using an inverted microscope.

Immunofluorescence (IF) staining

The appropriate density of cells was plated in a 6-well plate with glass slides. After the cells had adhered, the medium was replaced with drug-treated medium, and the cells were cultivated in an incubator. After the indicated time, the treated cells were fixed with 4% paraformaldehyde for 20 min. The fixed cells were permeabilized with 0.2% Triton X-100 for 5 min. Thereafter, the cells were incubated with the corresponding primary antibodies at 4 °C overnight. The corresponding secondary antibodies were incubated at room temperature for 1 h. During all the intervals between the transition processes, the cells were washed with PBS three times. An immunofluorescence staining kit (Beyotime) was used according to the protocol. Cell chromatin was stained with DAPI. Images were acquired with a Panoramic DESK (P-MIDI, P250; 3D HISTECH). Qupath software was used for the quantification in this study. For each treatment group, at least three microscopic areas were quantified.

SA-β-gal staining

Cells were plated at an appropriate density in a 6-well plate. After the cells had adhered, the medium was changed to drug-treated medium, and the cells were cultivated in an incubator for 48 h. Thereafter, the medium was removed, and the cells were washed once with PBS. One milliliter of β-galactosidase staining fixative was added to each well, after which the cells were fixed at room temperature for 15 min. The staining solution was removed, and the cells were washed three times with PBS. One milliliter of staining working solution was added to each well, after which the cells were incubated at 37 °C. After overnight incubation, an optical microscope was used to capture the stained cells.

Metabolite profiling and analysis

In this part, 1×10^4 cells per condition were pelleted and washed with precooled cold saline. The cell pellets were resuspended in 1 mL of 80% methanol solution containing 500 nM internal standards (Metabolomics Amino Acid Mix, Cambridge Isotope Laboratories, Inc.). The samples were vortexed at 4 °C and then centrifuged for 10 min. The supernatants were transferred, the samples were dried using a Speedvac, and then the samples were resuspended in 50 μL of high-performance liquid chromatography (HPLC)-grade water. Liquid chromatography–mass spectrometry (LC–MS) was performed using a mass spectrometer (Thermo Scientific™Dionex™MltiMate™3000 Rapid Separation LC (RSLC)) and a QExactive system. Specifically, samples were tested at multiple doses to ensure linearity of all metabolites. The specific operational approaches used referred to the manufactured protocols and previous related studies[18,41].

Flow cytometry

For cell cycle analysis, cells were seeded at an appropriate density and then treated with the designated drug concentrations. After 24 h, the treated cells were harvested and then fixed with precooled 70% ethanol at 4 °C overnight. The next day, the suspensions were centrifuged at $1000 \times g$ for 5 min to precipitate the cells, after which the supernatant was carefully removed. One milliliter of precooled PBS was used to resuspend the cells, after which the cells were centrifuged. Thereafter, 0.5 ml of propidium iodide staining solution (Lablead, Beijing, China) was added to each tube cell sample, which was subsequently incubated at 37 °C for 30 min in the dark. The results were analyzed on a FACSCalibur (BD Biosciences). For the cell apoptosis assay, an Annexin V-FITC apoptosis detection kit (Lablead) was used. The treated cells were stained according to the manufacturer's protocol. Apoptotic cells were detected on a FACSCalibur (BD Biosciences).

Immunohistochemistry (IHC)

Tissue slides were prepared following the methods described in our previous studies[12,20]. The corresponding primary antibodies and species-matched secondary antibodies were used in this part. The H score was used to evaluate the expression of cell cycle-related proteins. The slides were scanned by a Pannoramic Scanning Electron Microscope (3D HISTECH). The staining intensity was scored as 0, no staining; 1 point, weak intensity; 2 point, moderate intensity; 3 point, strong intensity[25,42]. H-score = (% weak intensity × 1) + (% moderate intensity × 2) + (% strong intensity × 3). The The final results were normalized to the control group for comparative analysis.

RNA-seq and analysis

Total RNA was isolated from treated cells with TRIzol (Invitrogen). RNA-seq and library preparation were conducted by Novogene using a paired-end sequencing pipeline. Paired-end reads were produced on the Illumina HiSeq 2500 platform. After quality control, the clean data were adjusted to the UCSC hg19 reference by STAR and measured using RSEM with default parameters. Genes with differential expression were identified with the R package DESeq2 (RRID:SCR_000154). Pathway enrichment analysis and gene set enrichment analysis (GSEA) were performed using the ClusterProfiler (RRID:SCR_016884) package.

Public datasets

Genomic and transcriptomic datasets obtained from the Cancer Genome Atlas Program (TCGA) database. The cell line information was downloaded from the cBioPortal platform. Pancancer genomic dependency data were downloaded from the DepMap portal. IHC staining results of SHMT were acquired from the Human Protein Atlas. The survival data of the genes were downloaded from the Kaplan–Meier Plotter.

Establishment of a subcutaneous tumor model in nude mice

Four-week-old male BALB/c nude mice were obtained from Charles River Company (Beijing, China). The nude mice were housed in a specific pathogen-free (SPF) animal room, and their growth, activity, body weight, and changes in implanted tumor volume were regularly monitored and measured. The entire experiment was approved and supervised by the Animal Care and Use Committee at Peking University First Hospital (Approval No: J2023034). The experimental procedures were conducted in accordance with the Animal Research: Reporting of In Vivo Experiments (ARRIVE) guidelines.

To establish the subcutaneous tumors model, 5×10^6 luc-HGC-27 cells were injected into the mice. The tumor dimensions were measured using manual palpation and digital callipers every 3 days. When the tumor volume reached 100–150 mm^3, the method of randomly assigning numbers divides mice into four groups (5 mice in each group) for regular intraperitoneal injection 3 times/week with (1) vehicle, (2) SHIN1 100 mg/kg, (3) 5-fu 10 mg/kg, or (4) the combination of 100 mg/kg SHIN1 with 10 mg/kg 5-fu[13,18,43]. The treatment experiment continued for 28 days. Tumor volumes

were measured using the following method: tumor volume = (longest diameter × shortest diameter^2)/2. After treatment was complete, the mice were imaged using an in vivo imaging system (PerkinElmer, USA). In vivo imaging procedures were conducted under anesthesia induced and maintained with isoflurane (3% for induction, 1.5% for maintenance via inhalation) in accordance ARRIVE guidelines. Thereafter, the tumors were harvested from the mice, measured, weighed, and photographed. The tumor cells extracted from the xenografts were further subjected to drug resistance experiments. We established two distinct cell line models through primary culture of gastric cancer specimens: 5-Fluorouracil-sensitive HGC-27/S cells derived from vehicle-treated tumors, and their chemoresistant counterpart HGC-27/R cells developed from 5-Fu-exposed tumor tissues. After experiments finish, euthanasia was performed by cervical dislocation for mice, a method consistent with ARRIVE guidelines. The statistical analysis and comparison were conducted with Prism software.

Statistical analysis

SPSS 25.0 and Prism 8.0 software were used to conduct the statistical analyses. The data are presented as the mean ± standard deviation (SD). Student's *t* test or the Wilcoxon test was used for statistical comparisons between groups. A two-tailed P value < 0.05 was regarded as statistically significant.

Data availability

Data are available from corresponding authors from reasonable request. The RNA sequencing data were submitted in NCBI database (https://www.ncbi.nlm.nih.gov/sra/PRJNA1229428).

Code availability

This study utilized the Xiantao Academic online platform (https://www.xiantao.love/) for statistical analysis and figure generation. The platform is built on R software 4.2.1 with pre-installed packages including ggplot2 3.4.4, stats 4.2.1, and car 3.1-0. No custom code was generated. Detailed information regarding all software versions and specific analysis parameters could request from Yisheng Pan (BDYYpanyisheng@163.com).

Received: 10 September 2024; Accepted: 24 April 2025;
Published online: 09 May 2025

References

1. Smyth, E. C., Nilsson, M., Grabsch, H. I., van Grieken, N. C. & Lordick, F. Gastric cancer. *Lancet* **396**, 635–648 (2020).
2. Sung, H. et al. Global Cancer Statistics 2020: GLOBOCAN Estimates of Incidence and Mortality Worldwide for 36 Cancers in 185 Countries. *CA Cancer J. Clin.* **71**, 209–249 (2021).
3. Parsa, S. et al. The serine hydroxymethyltransferase-2 (SHMT2) initiates lymphoma development through epigenetic tumor suppressor silencing. *Nat. Cancer* **1**, 653–664 (2020).
4. Liu, C. et al. Cytoplasmic SHMT2 drives the progression and metastasis of colorectal cancer by inhibiting beta-catenin degradation. *Theranostics* **11**, 2966–2986 (2021).
5. Morscher, R. J. et al. Mitochondrial translation requires folate-dependent tRNA methylation. *Nature* **554**, 128–132 (2018).
6. Ma, E. H. et al. Serine Is an Essential Metabolite for Effector T Cell Expansion. *Cell Metab.* **25**, 345–357 (2017).
7. Locasale, J. W. Serine, glycine and one-carbon units: cancer metabolism in full circle. *Nat. Rev. Cancer* **13**, 572–583 (2013).
8. Lewis, K. L. et al. High-Dose Methotrexate as CNS Prophylaxis in High-Risk Aggressive B-Cell Lymphoma. *J. Clin. Oncol.* **41**, 5376–5387 (2023).
9. Ong, Y. S., Banobre-Lopez, M., Costa, L. S. & Reis, S. A multifunctional nanomedicine platform for co-delivery of methotrexate and mild hyperthermia towards breast cancer therapy. *Mat. Sci. Eng. C. Mater.* **116**, 111255 (2020).
10. Liu, Y. et al. High expression of SHMT2 is correlated with tumor progression and predicts poor prognosis in gastrointestinal tumors. *Eur. Rev. Med. Pharmacol.* **23**, 9379–9392 (2019).
11. Zhao, M. et al. Drosha-independent miR-6778-5p strengthens gastric cancer stem cell stemness via regulation of cytosolic one-carbon folate metabolism. *Cancer Lett.* **478**, 8–21 (2020).
12. Nguyen, T. H. et al. Serine hydroxymethyltransferase 2 expression promotes tumorigenesis in rhabdomyosarcoma with 12q13-q14 amplification. J. Clin. Invest. 131, e138022 (2021).
13. He, L. et al. Suppression of nuclear GSK3 signaling promotes serine/one-carbon metabolism and confers metabolic vulnerability in lung cancer cells. *Sci. Adv.* **8**, m8786 (2022).
14. Garcia-Canaveras, J. C. et al. SHMT inhibition is effective and synergizes with methotrexate in T-cell acute lymphoblastic leukemia. *Leukemia* **35**, 377–388 (2021).
15. Dekhne, A. S. et al. Novel Pyrrolo[3,2-d]pyrimidine Compounds Target Mitochondrial and Cytosolic One-carbon Metabolism with Broad-spectrum Antitumor Efficacy. *Mol Cancer Ther.* **18**, 1787–1799 (2019).
16. Makino, Y. et al. Serine hydroxymethyltransferase as a potential target of antibacterial agents acting synergistically with one-carbon metabolism-related inhibitors. *Commun. Biol.* **5**, 619 (2022).
17. Wang, F. H. et al. The Chinese Society of Clinical Oncology (CSCO): Clinical guidelines for the diagnosis and treatment of gastric cancer, 2021. *Cancer Commun.* **41**, 747–795 (2021).
18. Pikman, Y. et al. Targeting serine hydroxymethyltransferases 1 and 2 for T-cell acute lymphoblastic leukemia therapy. *Leukemia* **36**, 348–360 (2022).
19. Beels, L., Bacher, K., De Wolf, D., Werbrouck, J. & Thierens, H. gamma-H2AX foci as a biomarker for patient X-ray exposure in pediatric cardiac catheterization: are we underestimating radiation risks?. *Circulation* **120**, 1903–1909 (2009).
20. Xiang, X. et al. Cellular senescence in hepatocellular carcinoma induced by a long non-coding RNA-encoded peptide PINT87aa by blocking FOXM1-mediated PHB2. *Theranostics* **11**, 4929–4944 (2021).
21. Yu, M. et al. Effect of epiberberine from Coptis chinensis Franch on inhibition of tumor growth in MKN-45 xenograft mice. *Phytomedicine* **76**, 153216 (2020).
22. Zhang, L. et al. Arsenic sulfide, the main component of realgar, a traditional Chinese medicine, induces apoptosis of gastric cancer cells in vitro and in vivo. *Drug Des. Devel Ther.* **9**, 79–92 (2015).
23. Isermann, T. et al. Suppression of HSF1 activity by wildtype p53 creates a driving force for p53 loss-of-heterozygosity. *Nat. Commun.* **12**, 4019 (2021).
24. Chen, Y., Yang, R., Guo, P. & Ju, Z. Gadd45a deletion aggravates hematopoietic stem cell dysfunction in ATM-deficient mice. *Protein Cell* **5**, 80–89 (2014).
25. Feng, M., Xu, H., Zhou, W. & Pan, Y. The BRD4 inhibitor JQ1 augments the antitumor efficacy of abemaciclib in preclinical models of gastric carcinoma. *J. Exp Clin. Canc. Res.* **42**, 44 (2023).
26. Zhou, M. et al. Chitosan-Gelatin-EGCG Nanoparticle-Meditated LncRNA TMEM44-AS1 Silencing to Activate the P53 Signaling Pathway for the Synergistic Reversal of 5-FU Resistance in Gastric Cancer. *Adv. Sci.* **9**, e2105077 (2022).
27. Yang, M. & Vousden, K. H. Serine and one-carbon metabolism in cancer. *Nat. Rev. Cancer* **16**, 650–662 (2016).
28. Ducker, G. S. et al. Human SHMT inhibitors reveal defective glycine import as a targetable metabolic vulnerability of diffuse large B-cell lymphoma. *Proc. Natl. Acad. Sci. USA* **114**, 11404–11409 (2017).
29. Zhang, Y. et al. SHMT2 promotes cell viability and inhibits ROS-dependent, mitochondrial-mediated apoptosis via the intrinsic signaling pathway in bladder cancer cells. *Cancer Gene Ther.* **29**, 1514–1527 (2022).

30. Paone, A. et al. SHMT1 knockdown induces apoptosis in lung cancer cells by causing uracil misincorporation. *Cell Death Dis.* **5**, e1525 (2014).
31. Shi, H., Fang, X., Li, Y. & Zhang, Y. High Expression of Serine Hydroxymethyltransferase 2 Indicates Poor Prognosis of Gastric Cancer Patients. *Med. Sci. Monitor.* **25**, 7430–7438 (2019).
32. Ye, H. et al. PICH Activates Cyclin A1 Transcription to Drive S-Phase Progression and Chemoresistance in Gastric Cancer. *Cancer Res.* **83**, 3767–3782 (2023).
33. Poursheikhani, A. et al. Non-coding RNAs underlying chemoresistance in gastric cancer. *Cell Oncol.* **43**, 961–988 (2020).
34. Huang, S. et al. The UbL-UBA Ubiquilin4 protein functions as a tumor suppressor in gastric cancer by p53-dependent and p53-independent regulation of p21. *Cell Death Differ.* **26**, 516–530 (2019).
35. Zhu, Y. et al. Adenovirus-directed expression of TIPE2 suppresses gastric cancer growth via induction of apoptosis and inhibition of AKT and ERK1/2 signaling. *Cancer Gene Ther.* **23**, 98–106 (2016).
36. Imanishi, M. et al. Augmented antitumor activity of 5-fluorouracil by double knockdown of MDM4 and MDM2 in colon and gastric cancer cells. *Cancer Sci.* **110**, 639–649 (2019).
37. Hamilton, E. & Infante, J. R. Targeting CDK4/6 in patients with cancer. *Cancer Treat Rev.* **45**, 129–138 (2016).
38. Chen, Z. et al. Pyrotinib combined with CDK4/6 inhibitor in HER2-positive metastatic gastric cancer: A promising strategy from AVATAR mouse to patients. *Clin. Transl. Med.* **10**, e148 (2020).
39. Alves, C. L. et al. Co-targeting CDK4/6 and AKT with endocrine therapy prevents progression in CDK4/6 inhibitor and endocrine therapy-resistant breast cancer. *Nat. Commun.* **12**, 5112 (2021).
40. Christensen, S. et al. 5-Fluorouracil treatment induces characteristic T>G mutations in human cancer. *Nat. Commun.* **10**, 4571 (2019).
41. Cortese, M. et al. Validation of a LC/MSMS method for simultaneous quantification of 9 nucleotides in biological matrices. *Talanta* **193**, 206–214 (2019).
42. Deng, H. et al. LncRNA CCAT2 promotes malignant progression of metastatic gastric cancer through regulating CD44 alternative splicing. *Cell Oncol.* **46**, 1675–1690 (2023).
43. Wang, X. et al. Gastric cancer vaccines synthesized using a TLR7 agonist and their synergistic antitumor effects with 5-fluorouracil. *J. Transl. Med.* **16**, 120 (2018).

Acknowledgements

This study was funded by National Natural Science Foundation of China (Approval No. 81970459).

Author contributions

All authors contributed to the study conception and design. Huan Deng designed the study and Yisheng Pan supervised the process of research. Huan Deng, Yajie Wang and Mei Feng performed the experiments, collected data, and wrote the original draft. Lin Xiao and Weidong Dou analyzed and visualized the data. Randomization and blinding of the entire experiment arrange by Mei Feng. All authors contributed to this research and approved the final version.

Competing interests

The authors declare no competing interests.

Additional information

Supplementary information The online version contains supplementary material available at https://doi.org/10.1038/s41698-025-00926-5.

Correspondence and requests for materials should be addressed to Yisheng Pan.